

Published online in Science Express (26 Feb. 2004)

To appear in print in Science (2004)

Discovery of a large dust disk around the nearby star AU Microscopium

Paul Kalas^{1,2}, Michael C. Liu³, Brenda C. Matthews¹

ABSTRACT

We present the discovery of a circumstellar dust disk surrounding AU Microscopium (AU Mic, GJ 803, HD 197481). This young M star at 10 parsec has the same age and origin as ρ Pictoris, another nearby star surrounded by a dust disk. The AU Mic disk is detected between 50 AU and 210 AU radius, a region where dust lifetimes exceed the present stellar age. Thus, AU Mic is the nearest star where we directly observe the solid material required for planet formation. Since 85% of stars are M-type, the AU Mic disk provides new clues on how the majority of planetary systems might form and evolve.

1. Introduction

About 15% of nearby main-sequence stars exhibit an excess of far-infrared radiation that points to the existence of circumstellar dust grains (1). Dust grains have short lifetimes, and their continued presence implies a source of replenishment. The solar system has a disk-like distribution of dust that is continually replenished by the sublimation of comets and collisions between asteroids. We therefore infer that similar populations of undetected parent bodies produce dusty debris disks around infrared excess stars. Moreover, evidence for planets can be found by matching density variations in debris disks to theoretical models of how planets gravitationally perturb these disks (2, 3, 4). In effect, circumstellar debris disks are a signpost for the existence of extrasolar planetary systems.

¹Astronomy Department and Radio Astronomy Laboratory, 601 Campbell Hall, Berkeley, CA 94720

²National Science Foundation Center for Adaptive Optics, University of California, Santa Cruz, CA 95064

³Institute for Astronomy, 2680 Woodlawn Dr., Honolulu, HI 96822

Direct images of debris disks are rare. Starlight reflecting off optically thin debris disks is detected at optical and near-infrared wavelengths in only three cases – Pictoris, HR 4796A and HD 141569 (5, 6, 7). In three more cases – Vega, Fomalhaut, and Eridani – debris disk structure is seen only at thermal infrared wavelengths (8, 9). Pictoris, HR 4796A and HD 141569 are relatively young (< 20 Myr) main sequence stars that have the largest disk masses, and hence represent the more detectable of the debris disk systems.

Pictoris has Galactic space motions in common with two M stars, AU Mic and AT Mic, that have ages \sim 20 Myr (10). These stars and Pictoris may be co-eval sister stars that have separated in space over time due to the small differences in their space motions. A total of 17 stars may be members of this group with age 8 ± 20 Myr (11). AU Mic has significant infrared excess at 60 μ m (12, 13) and recent sub-millimeter data reveal the presence of cold (40 K) dust, a total dust mass roughly three times smaller than that of Pictoris (Table 1), an absence of molecular gas, and a lack of grains within 17 AU of the star (14).

2. Observations

We endeavored to directly image circumstellar dust around AU Mic with an optical stellar coronagraph at the University of Hawaii 2.2-m telescope on Mauna Kea, Hawaii (15). The stellar coronagraph (Fig. S1) produces artificial eclipses of stars by blocking the light at the focal plane with a circular opaque mask suspended by four wires. Instrumental diffracted light is blocked by a Lyot mask in the pupil plane. The net result is significantly enhanced contrast in the regions surrounding bright stars. The imaging camera behind the coronagraph is a Tek 2048 \times 2048 CCD with a scale of $0.41''/\text{pixel}$. All our data were obtained through a standard broadband R filter ($\lambda_c = 647 \text{ nm}$, $\Delta\lambda = 125 \text{ nm}$).

We acquired data on 14 and 15 October, 2003, with $6.5''$ and $9.5''$ diameter occulting spots, respectively. We obtained five 240-s and three 300-s images of AU Mic on the first and second nights, respectively. In addition to AU Mic, we observed five other bright stars to check for spurious features such as diffraction spikes and internal reflections (Table S1). A disk-like reflection nebulosity surrounding AU Mic was detected in raw data during both nights of observation and does not match the position angle (PA, measured east from north), width, or morphology of instrumental diffraction spikes. The image quality as measured by the full-width at half maximum (FWHM) of field stars was $1.1''$.

Data reduction followed the standard steps of bias subtraction, flat-fielding and sky-subtraction. We then subtracted the stellar point spread function (PSF) to remove excess stellar light from around the occulting spot. We used the real PSFs from other stars observed

throughout each night, as well as artificial PSF's. Artificial PSF subtraction is effective for AU Mic because the circumstellar disk is close to edge-on. We extracted the stellar PSF for each image of AU Mic by sampling the image radially in a direction perpendicular to the PA of the disk. We then fit a polynomial to the data and generated an artificial PSF that is a figure of rotation of the polynomial. The PSF's were then scaled and registered to each data frame such that subtraction minimized the residual light in directions perpendicular to the disk beyond the edge of the occulting spot. In general, the different PSF subtractions produce comparable results, with minor differences appearing a few pixels beyond the edge of the occulting spot. To evaluate the uncertainties in our final image, we measured disk properties in four different data sets that represent two nights of observation, and each with two different PSF subtraction techniques. The data for Pic from (16) that are discussed below were obtained with the same telescope, coronagraph, and filter, and analyzed using similar techniques.

3. Circumstellar Dust Morphology

The reflection nebulosity around AU Mic is consistent with a circumstellar disk seen at a near edge-on viewing geometry (Fig. 1, Fig. S2). We detect the disk as far as 21° (210 AU) from the star (17). This sensitivity-limited value is a lower limit to the true disk outer radius. The inner radius of the detected disk is 5° (50 AU) and is mainly limited by the radius of the occulting spot and artifacts of the PSF subtraction. The position angles of the two disk midplanes differ by about 6.3° ; PA = 124.2° for the SE side and PA = 310.1° for the NW side. A similar, $1.0 - 2.5^{\circ}$ offset, called the "wing-tilt asymmetry", was measured for the Pic midplanes (16). An asymmetric disk can appear to have a wing-tilt when the disk axis is tilted to the line of sight and the scattering phase function is non-isotropic. A model-dependent relationship between the observed wing-tilt and the intrinsic disk inclination (16) suggests that AU Mic disk is inclined $7 - 20^{\circ}$ from edge-on. On the other hand, the sharp midplane morphology is consistent with model disks that have inclinations no greater than 5° from edge-on (18, Fig. S3). Until higher resolution data are obtained and analyzed, we adopt a disk inclination of 5° from edge-on.

Power-law fits to the disk midplanes between 6° (60 AU) and 16° (120 AU) radius give indices of -3.6 and -3.9 for the NW and SE extensions, respectively (Fig. 2). These indices are similar to the power-law fits for the NE and SW disk extensions of Pic (Table 1) (16). However, the midplane profiles for Pic become less steep inward of 100 AU. No such turnover is seen for the AU Mic radial profiles. The NW midplane of AU Mic also shows a significant enhancement in surface brightness 9° radius from the star (Fig. 1, Fig. 2). This

could be due to a background source, but further tests using color, polarization and proper motion information should be evaluated before excluding a physical connection to AU Mic.

4. Discussion

The existence of morphologically similar dust disks around AU Mic and ρ Pic supports the hypothesis that these are sister stars born at the same time and location. However, the two disks are not twins. The total mass of dust estimated from the spectral energy distributions is 3.3 times greater for ρ Pic relative to AU Mic (Table 1). The relative brightnesses of the two disks in optical data are consistent with this result. To make the comparison, we imagine placing the ρ Pic dust disk around AU Mic. In Figure 2, we include the midplane surface brightness profile for ρ Pic using data from (16) that is now scaled by factors that account for the AU Mic heliocentric distance and stellar luminosity. We find that if the disk of ρ Pic surrounded AU Mic it would be about $1.5 \text{ mag arcsec}^{-2}$ brighter than what we measure for the AU Mic disk (Fig. 2). This corresponds to a factor of four greater scattering cross section of ρ Pic grains relative to AU Mic grains. If we assume that the two disks have exactly the same structure, grain properties, and viewing geometry then the AU Mic disk requires a dust mass that is four times smaller than that of ρ Pic. Future observations of disk properties such as the inclination of AU Mic will elucidate the validity of these assumptions, but this result is consistent with the infrared dust luminosity.

The underlying grain properties are also likely to differ due to the weak radiation environment of an M star relative to an A star. AU Mic is 3.6 times less massive than ρ Pic, and 87 times less luminous (Table 1). For the AU Mic disk, the collision timescale at 100 AU radius is $0.2 - 1.8 \text{ Myr}$ assuming a dust optical depth of $10^{-3} - 10^{-4}$, respectively (Fig. S4). At 200 AU, near the outer boundary of the detected disk, the collision timescale is $0.5 - 5.0 \text{ Myr}$. Given an age of $8 - 20 \text{ Myr}$ for AU Mic, most disk particles have undergone at least one collision. However, as objects are shattered into smaller pieces, the radiation pressure force around AU Mic is too weak to remove the fragments (19). They can be removed by the system either by joining together to form larger objects, or by spiraling into the star by Poynting-Robertson (PR) drag. The PR timescales at 100 AU are $0.2 - 1.8 \text{ Gyr}$ for $1 - 10 \mu\text{m}$ particles, respectively many times longer than the age of the system (1). For

ρ Pic, on the other hand, grains a few microns and smaller are quickly ejected by radiation pressure and the disk mass diminishes over time (20). The AU Mic disk should preserve a larger population of sub-micron sized grains, and the mass of solid objects observed today should approximate the primordial disk mass. In other words, most of the disk seen in our optical scattered light image may consist of primordial solid material.

Within 50 AU of the star, the timescales for grain removal by collisions and PR drag become significantly shorter than the stellar age. Primal dust at the inner limit of our images (Fig. 1, 2) has mostly vanished, and the grains observed here, as well as those discovered as close as 17 AU from the star (14), must be continually replenished by the collisional erosion of much larger objects such as comets and asteroids. The existence of planetesimals in this region lends plausibility to the argument that the same objects will form planets by accretion. Given that AU Mic is only 10 Myr old, we may be able to observe planets that are still in the process of accreting mass, or at least discern disk structure that is sculpted by planet-mass bodies. Because AU Mic is closer to the Sun than Pic, the 2–30 AU zone where terrestrial and gas giant planets might form can be resolved by current and future instrumentation (Fig. S5). Planets around AU Mic may also be detected by indirect methods. The low stellar mass means that the star will display a significant astrometric reflex motion (2 milli-arcsec for a Jupiter-analog). The near edge-on orientation favors planet detection by transits of the stellar photosphere. Finally, if a planet is detected by radial velocity techniques, then the near edge-on orientation gives the planet mass by constraining the $\sin(i)$ ambiguity intrinsic to these measurements.

References and Notes

1. D. E. Backman, F. Paresce, in *Protostars and Protoplanets III*, E. H. Levy and J. I. Lunine, Eds. (University of Arizona Press, Tucson, 1993), pp. 1253-1304.
2. F. Roques, H. Scholl, B. Sicardy, B. A. Smith, *Icarus* 108, 37 (1994).
3. J.-C. Liou, H. A. Zook, *Astron. J.* 118, 580 (1999).
4. L. M. Ozemoy, N. N. Gorkavyi, J. C. Mather, T. A. Taidakova *Astrophys. J.* 537, L147 (2000).
5. B. A. Smith, R. J. Terile, *Science* 226, 1421 (1984).
6. G. Schneider et al, *Astrophys. J.* 513, L127 (1999).
7. M. D. Silverstone et al, *Bull. Am. Astron. Soc* 30, 1363 (1998).
8. W. S. Holland et al, *Nature* 392, 788 (1998).
9. J. S. Greaves et al, *Astrophys. J.* 506, L133 (1998).
10. D. Barrado y Navascues, J. R. Staufer, I. Song, J.-P. Caillaud, *Astrophys. J.* 520, L123 (1999).
11. B. Zuckerman, I. Song, M. S. Bessell, R. A. Webb, *Astrophys. J.* 562, L87 (2001).
12. V. T sikoudi, *Astron. J.* 95, 1797 (1988).
13. I. Song, A. J. Weinberger, E. E. Becklin, B. Zuckerman, C. Chen, *Astron. J.* 124, 514 (2002).
14. M. C. Liu, B. C. Matthews, J. P. Williams, P. G. Kalas, *Astrophys. J.*, in press (2004).
15. Materials and methods are available as supporting material on Science Online.
16. P. Kalas, D. Jewitt, *Astron. J.* 110, 794 (1995).
17. To increase the signal-to-noise of the data shown in Fig. 1, we binned the data 3 × 3 pixels and then smoothed by a Gaussian function with $\sigma = 0.5$ pixel. This smoothed image was used to find the maximum outer extent of the disk. All other measurements were made using the unbinned and unsmoothed image shown in Fig. 1.
18. P. Kalas, D. Jewitt, *Astron. J.* 111, 1347 (1996).
19. R. Saija, et al. *Mon. Not. R. Astron. Soc.* 341, 1239 (2003).
20. P. Artymowicz, *Astrophys. J.* 335, L79 (1988).

21. M . S . Bessel, F . C astelli, B . P lez, *Astron. Astrophys.* 333, 231 (1998).
22. F . C rifo, A . V idalM adjar, R . L allen ent, R . Ferlet, M . G erbaldi, *Astron. Astrophys.* 333, L29 (1997).
23. J . D . Larwood, P . G . K alas, *Mon. Not. R . Astron. Soc.* 323, 402 (2001).
24. W . R . F . D ent, H . J . W alker, W . S . H olland, J . S . G reaves, *Mon. Not. R . Astron. Soc.* 314, 702 (2000).
25. This work has been supported by the NA SA O riginals P rogram under grant NA G 5-11769, and the NSF C enter for A daptive O ptics, m anaged by the U niversity of C alifornia at Santa Cruz under cooperative agreem ent No. A ST -9876783. BCM ackow ledges support from NSF grant # 0228963. M CL ackow ledges support from a Hubble Postdoctoral Fellowship (NA SA G rant H ST -HF -01152.01). The authors ackow ledge the insightful contributions of two anonym ous referees.

Supporting O nline M aterial

[www .science.org](http://www.science.org)

M aterials and M ethods

Figs. S1, S2, S3, S4 and S5

Table S1

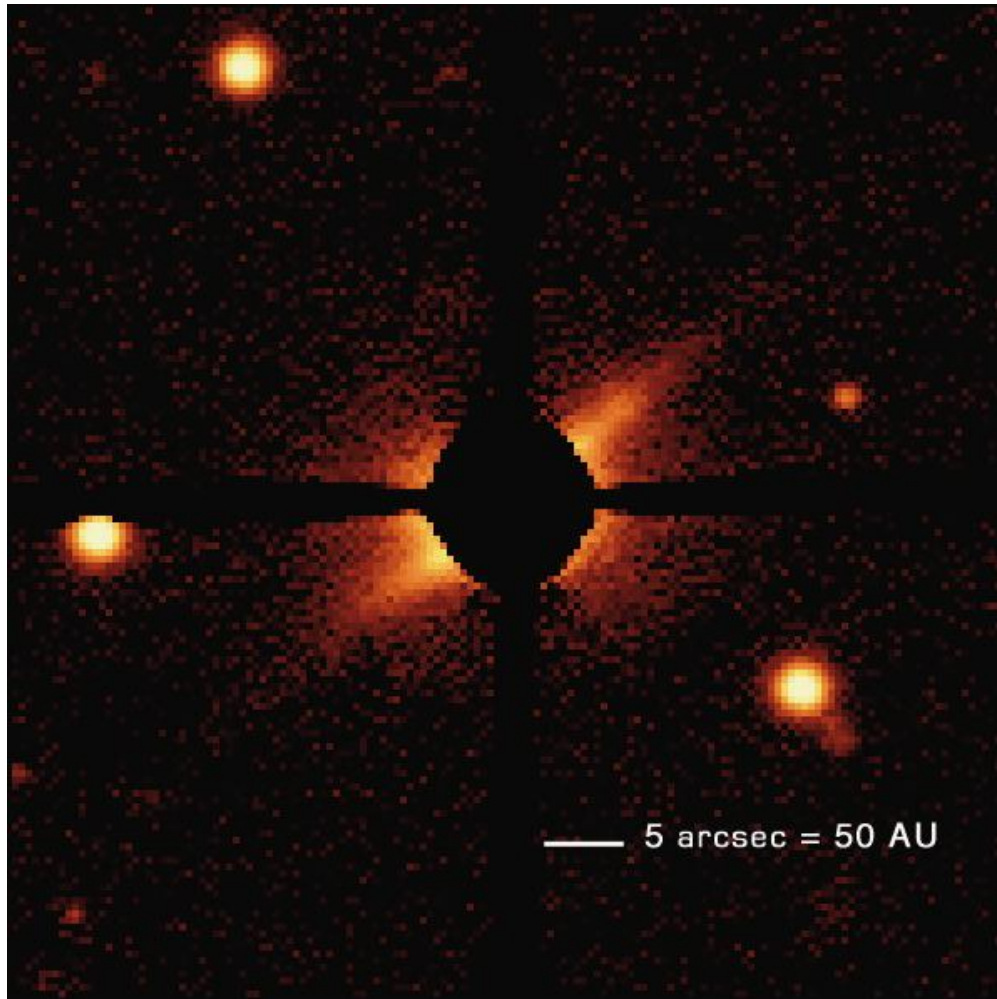


Fig. 1. The disk surrounding AU Mic seen in optical scattered light. North is up, east is left, and each side of this false-color image corresponds to $60''$. The central dark region is produced by the $9.5''$ diameter focal plane occulting spot which is suspended by four wires and completely masks our direct view of the star. This image represents 900 seconds total integration in the R band and each pixel corresponds to 4 AU at the distance to AU Mic. Residual light evident near the occulting spot edge in the NE-SW direction is attributed to asymmetries in the point-spread function caused by instrumental scattering and atmospheric seeing.

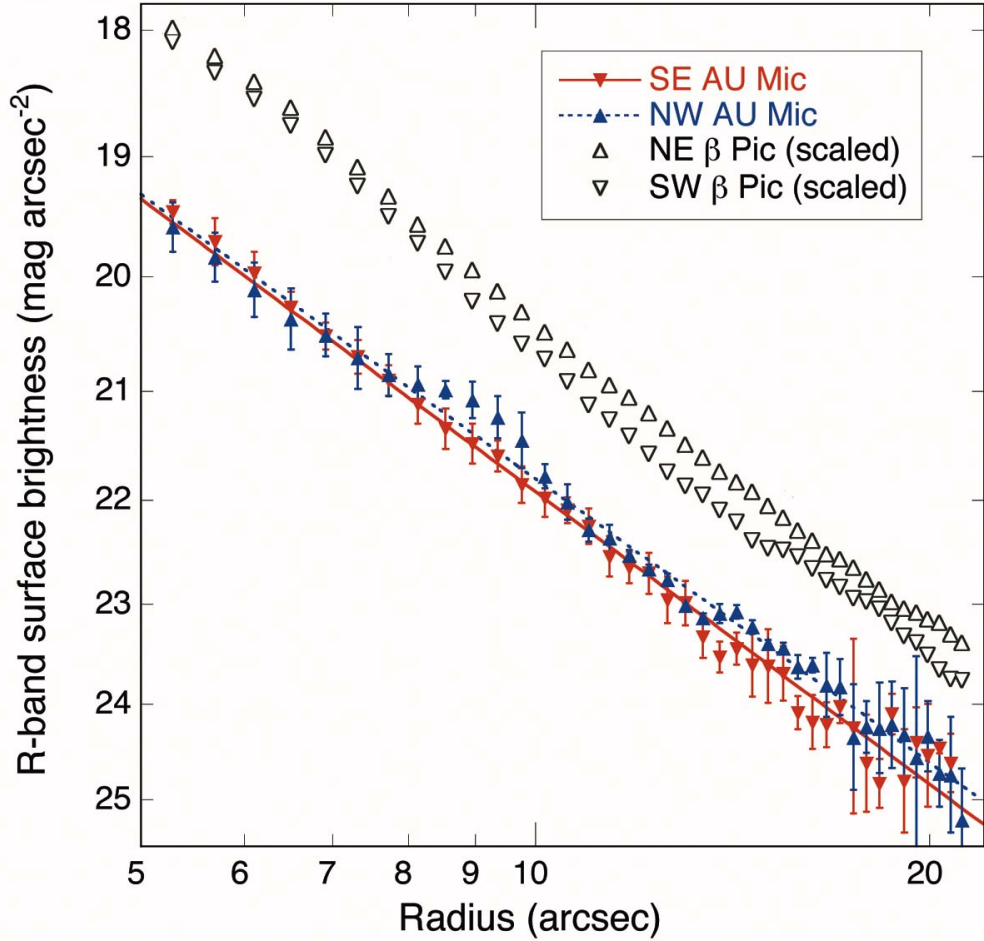


Fig. 2. | Midplane surface brightness as a function of radius. The midplane was sampled between 5° and 21° radius along a strip 1.2° wide. We show the mean value from two nights of data with two different PSF subtraction techniques. The error bars represent one standard deviation of a single measurement. We fit the data between 6° and 16° radius with power laws that give indices -3.6 and -3.9 for the NW and SE midplanes of AU Mic, respectively. The radial profile for the NW midplane has a significant brightness enhancement at 9° radius that is either intrinsic to the disk or a background object. We also plot the surface brightness of the Pic disk from (16), but with the surface brightness uniformly $3.0 \text{ mag arcsec}^{-2}$ fainter to simulate the existence of Pic's disk around AU Mic at 9.9 pc . This scaling takes into account the fact that the absolute R-band magnitude of AU Mic is 5.6 mag fainter than Pic (Table 1), and at a constant angular radius the Pic disk is roughly a factor of $(d_{\text{AU Mic}}/d_{\text{Pic}})^{3.6} = (9.9/19.3)^{3.6} = 11.3$ times brighter (i.e. 2.6 mag brighter; see Eqn. 4 in 18).

Table 1. Star (rows 1-8) and disk (rows 9-13) properties for AU Mic and Pic. The stellar parameters for AU Mic are derived from data given by (10, 13, 21). For Pic's stellar parameters, we use (22) and references therein. The Pic disk R-band surface brightness (SB) at 6^{th} radius is given in (16), while its maximum extent is given in (23).

	AU Mic	Pic
Spectral Type	M 1Ve	A 5V
Mass (M_{\odot})	0.5	1.8
T_{eff} (K)	3500	8200
Luminosity (L_{\odot})	0.1	8.7
Distance (pc)	9.9	19.3
V (mag)	8.8	3.9
M_V (mag)	8.8	2.4
V-R	0.88	0.08
Disk SB (6^{th})	20.1 \pm 0.3	15.4 \pm 0.3
SB fall-off ^a	-3.6 to -3.9	-3.8 to -4.1
Max. Radius (AU)	210	1835
$= L_{\text{disk}}/L_{\text{bol}}^{\text{b}}$	6.1×10^{-4}	3×10^{-3}
Total Dust Mass (g) ^c	6.6×10^{25}	2.2×10^{26}

^aValue of exponent for a power-law fit to disk R-band surface brightness fall-off between 6 - 16^{th} radius. The shallower surface brightness profiles correspond to the NW and NE brightness profiles of AU Mic and Pic, respectively. The Pic values are taken from (16).

^bThe fractional dust luminosity, assuming an optically thin disk, determined by taking the ratio of excess infrared luminosity to stellar bolometric luminosity. The values are obtained from (14) and (1) for AU Mic and Pic, respectively.

^cDust mass from models to the spectral energy distribution taken from (14) for AU Mic, and (24) for Pic.

SUPPORTING ONLINE MATERIAL
Materials and Methods

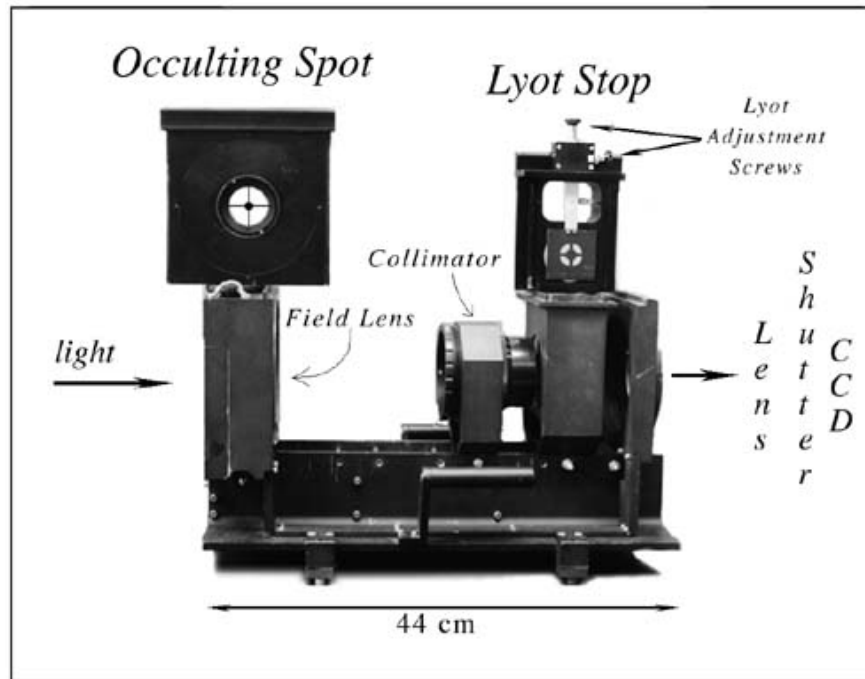


Fig. S1: The optical stellar coronagraph used for these observations. The main function of a stellar coronagraph is to block light from a bright star in order to detect faint, nearby objects. The occulting spot is placed at the focal plane of the telescope and prevents light from striking any optical elements further down in the optical path. Without the occulting spot, light from the star would saturate the CCD, and the optical elements would fill the background with scattered light, as well as produce spurious reflections. The optical elements in the coronagraph are used to create an image of the pupil plane, essentially an image of the telescope mirrors, and support structures. The Lyot stop is appropriately shaped to block this image of the telescope diffraction pattern – stars imaged with a coronagraph do not have diffraction spikes. The removal of the diffraction pattern is a major advantage when trying to image faint sources near the star.

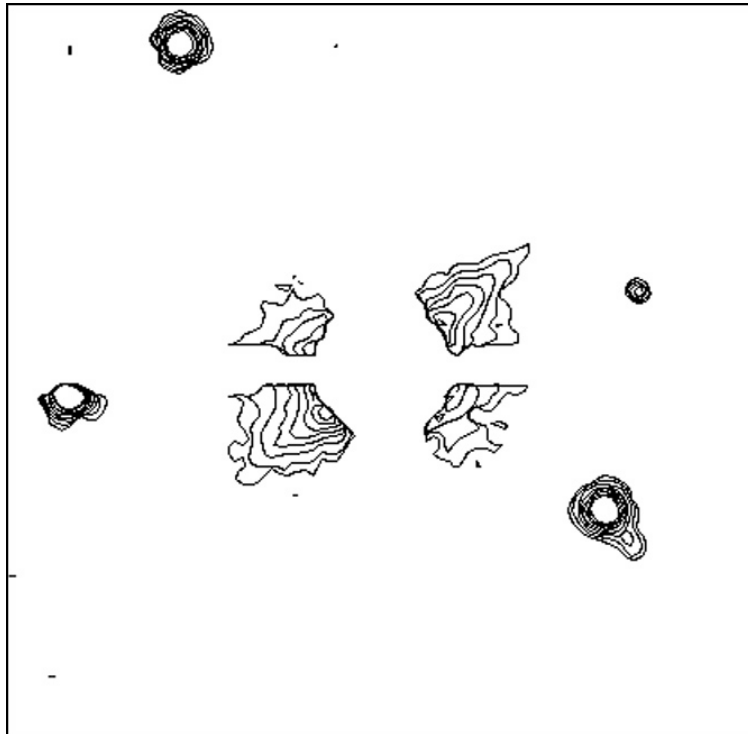


Fig. S2: R-band surface brightness maps corresponding to Fig. 1. Isophotes are plotted at $0.5 \text{ mag arcsec}^{-2}$ intervals from 23.5 to $20.0 \text{ mag arcsec}^{-2}$. As with Fig. 1, north is up, east is left, and the sides of the box represent $60''$.

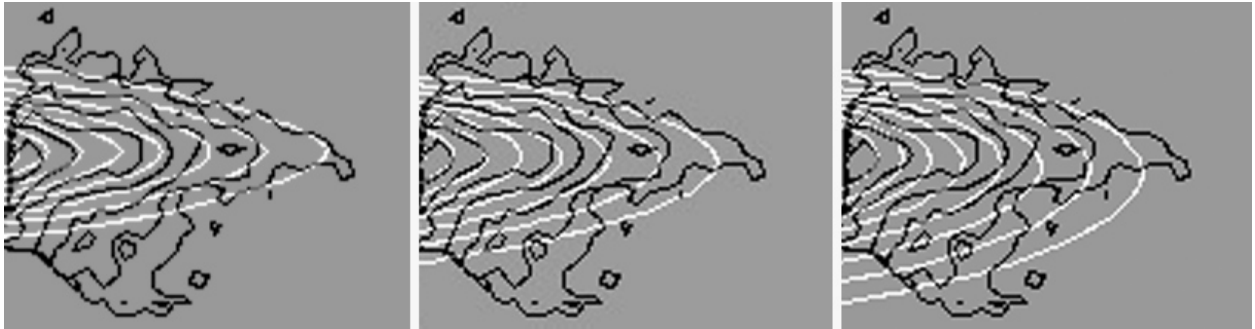


Fig. S3: Comparison of the AU Mic disk to model disks at different inclinations to the line of sight. We rotate the surface brightness map of AU Mic such that the midplane of the NW disk extension is oriented horizontally (black contours). The three panels above show a model disk (white contours) that is inclined edge-on (left panel), 5° from edge-on (middle panel), and 10° from edge-on (right panel). The model used is identical to the Pic model described in Section 4.1 of (1). It is normalized to the AU Mic surface brightness at $6''$ radius (Fig. 2), and convolved with a Gaussian to simulate the seeing conditions during the observations. In the dust disk model, the midplane volume number density distribution decreases with radius as a power-law with index -2.6 . All model parameters are kept the same in the three models above, except for the disk inclination to the line of sight. Our main conclusion is that the AU Mic disk strongly resembles the Pic disk in its morphology and disk inclination. The model that is 10° away from edge-on (right panel) demonstrates isophotes that are significantly more rounded at the midplane than what we observe for AU Mic. Thus, given the limited $1.1''$ resolution of our observations, we constrain the disk inclination to no greater than 5° from edge-on.

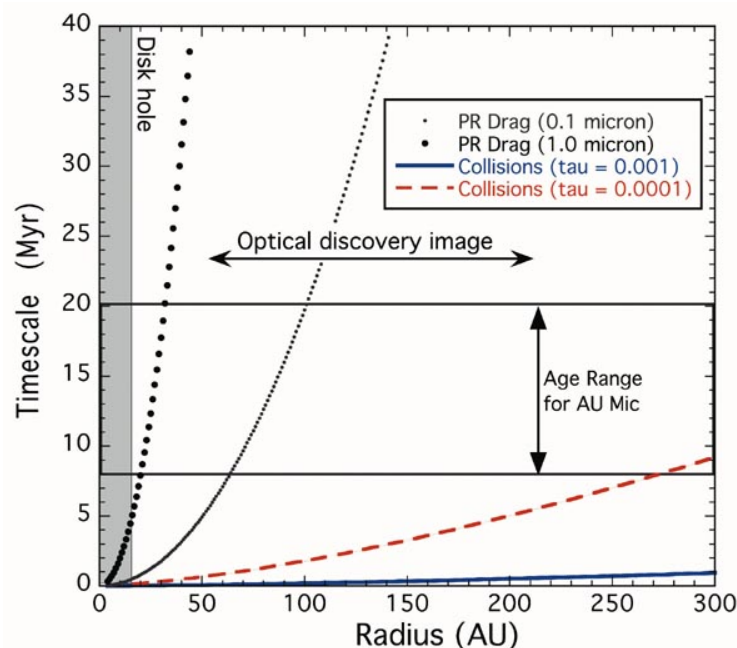


Fig. S4: Dust lifetimes as a function of radius. After gas in a circumstellar disk has dispersed, and the system becomes optically thin, Poynting-Robertson (PR) drag causes grains to spiral into the star. Using the equation for PR drag timescales given by (2), we plot the PR drag timescales for 0.1 μm and 1.0 μm grains. At radii < 67 AU, the 0.1 μm grains have spiraled into the star by 8 Myr. The 1.0 μm grains, on the other hand, take much longer to spiral into the star if they are initially located at 67 AU radius. In fact, only if they were within ~ 20 AU radius would 1.0 μm grains have enough time (8 Myr) to spiral into the star. In the region between 20–67 AU we would expect to find a lack of 0.1 μm grains. Beyond 67 AU, the 0.1 μm grains have not had enough time to spiral into the star. The disk scattered light may appear bluer at these larger radii due to Rayleigh scattering. The collision timescales are also shown (2). We assume two values for optical depth, τ , that span a likely range of values inferred from the observed spectral energy distribution (Table 1). At 100 AU radius, and for $\tau = 0.0001$, the collision timescale is 1.8 Myr. If the age is 8 Myr, then grains are likely to have had at least one collision. Collisions tend to be destructive, increasing the population of submicron grains. Thus most of the grains seen in the discovery image (Fig. 1) are pieces of larger objects, and this is why such disks are called "debris disks". Unlike very luminous stars such as β Pic and Vega, the submicron grains orbiting AU Mic will not be ejected outward by radiation pressure. Therefore, the disk around AU Mic should retain a larger fraction of its primordial material. Beyond ~ 200 AU radius we expect the disk to be collisionally un-evolved. The grains here may represent the pristine material in interstellar clouds that are the building blocks for larger particles that join to form planetesimals such as comets and asteroids. Also shown above is a gray region that indicates the inferred radius of a hole in the disk (3). The force of PR drag discussed above should cause grains to spiral into this region from the outer parts of the disk. The fact that very warm material is not evident at infrared wavelengths indicates that grains are prevented from approaching closer than ~ 17 AU radius. The existence of the hole hints at the possibility of a planet-mass object orbiting the star because planet-grain encounters are one mechanism for efficient grain removal.

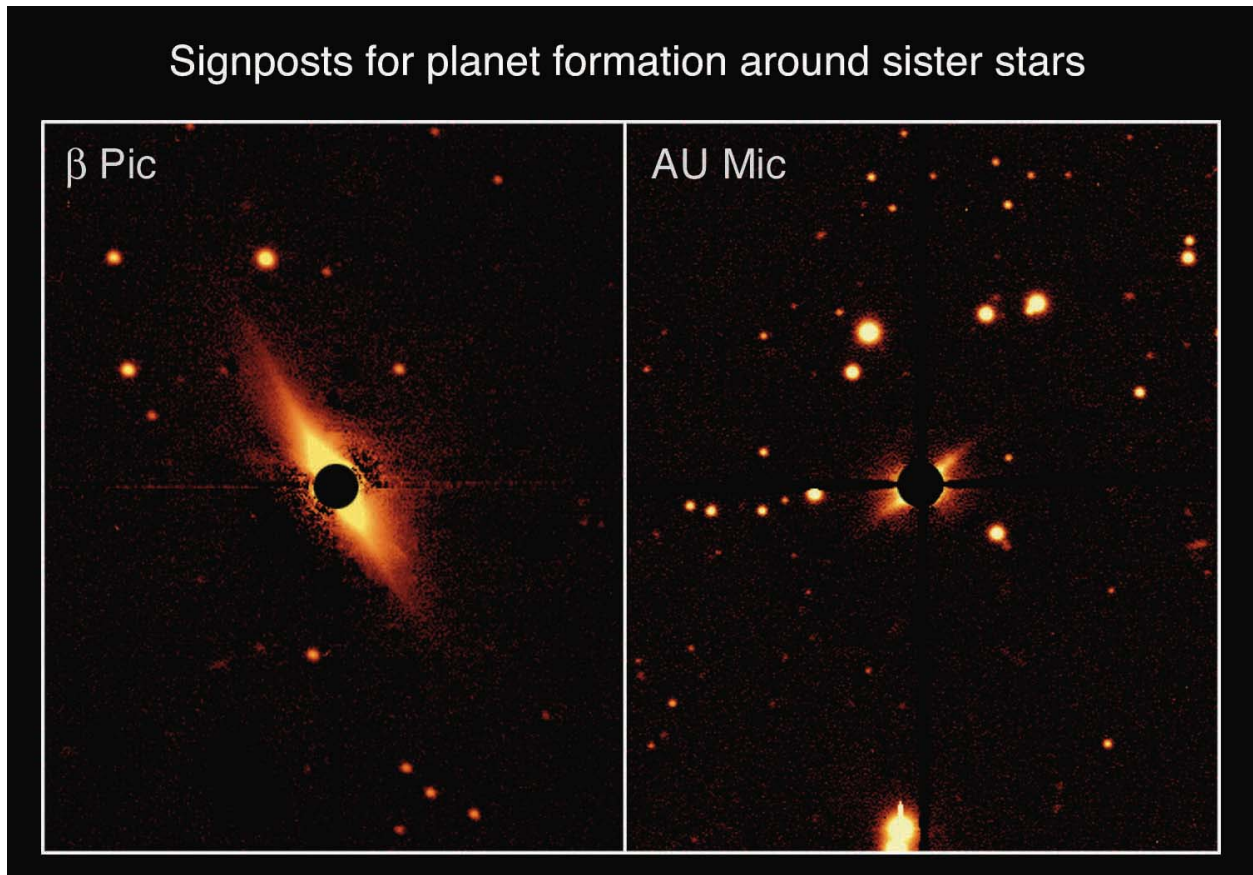


Fig. S5: Beta Pic on the left (4) was imaged with the same telescope, filter, and instrument as AU Mic on the right (this paper). The total integration times are nearly equal, providing roughly the same sensitivity. The β Pic disk appears brighter because it surrounds a brighter star, and it contains more dust grains than the AU Mic disk. These false-color images are also shown to the same angular scale – the circular black masks have diameter $10''$. Because β Pic is about twice as distant as AU Mic is, $10''$ corresponds to 193 astronomical units at β Pic, and only 99 astronomical units at AU Mic. Therefore, in the case of AU Mic, the dust disk observed near the boundary with the black mask approximately corresponds to the Kuiper Belt in our solar system. The proximity and youth of AU Mic make it an ideal target to directly study the possible planet-forming environment hidden behind the mask used in our observations. Ground-based telescopes with adaptive optics and the Hubble Space Telescope are well suited for examining this region. Together, AU Mic and β Pic present an exciting opportunity to understand how two planetesimal systems born at the same time will evolve differently.

References for the Supporting Online Material

1. P. Kalas, D. Jewitt, *Astron. J.* 111, 1347 (1996).
2. D. E. Backman, F. Paresce, in *Protostars and Protoplanets III*, E. H. Levy and J. I. Lunine, Eds. (University of Arizona Press, Tucson, 1993), pp. 1253-1304.
3. M. C. Liu, B. C. Matthews, J. P. Williams, P. G. Kalas, *Astrophys. J.*, in press (2004).
4. P. Kalas, D. Jewitt, *Astron. J.* 110, 794 (1995).

Table S. 1 : PSF reference stars used in the analysis of the AU Mic data

Name	RA (J2000)	DEC (J2000)	V (mag)	SpT
HD 17925	02 52 32	-12 46 10	6.0	K 1V
HD 22049	03 32 56	-09 27 30	3.7	K 2V
HD 193281	20 20 28	-29 11 50	6.3	A 2III
HD 207129	21 48 15	-47 18 13	5.6	G 0V
HD 216489	22 53 02	+ 16 50 28	5.9	K 1.5II-IIIe